Journal of Drug Delivery Science and Technology 101 (2024) 106282

Contents lists available at ScienceDirect

Journal of Drug Delivery Science and Technology

journal homepage: www.elsevier.com/locate/jddst

On the axonal transport of lipid nanoparticles in primary hippocampal neurons

Ana M. Martins [a], Roberto Palomba [a,*], Michele Schlich [b], Paolo Decuzzi [a]

[a] Laboratory of Nanotechnology for Precision Medicine, Istituto Italiano di Tecnologia, Via Morego 30, 16163, Genova, Italy
[b] Department of Life and Environmental Sciences, University of Cagliari, 09124, Cagliari, Italy

A B S T R A C T

Axonal transport is a crucial process in healthy neurons as it supports the intra-cellular movement of nutrients, endogenous substances, and vesicles regulating a broad set of biological functions. Notably, this physiological mechanism is efficiently exploited by a variety of viruses to infect multiple cells within the central nervous system and, thus, it has been proposed as a strategy to enhance the brain penetrance of macromolecules and nanoparticles. In this work, the retrograde and anterograde transport of lipid nanoparticles (LNP) is systematically analyzed in primary hippocampal neurons cultured in compartmentalized microfluidic chips, where neurites are left to grow within 150 μm-long channels connecting the somal and synaptic compartments. After characterizing the physico-chemical properties, toxicological profile, and cell internalization efficiency, the axonal trafficking of fluorescently labeled LNP was monitored over time via live-cell microscopy. Both naïve LNP and apolipoprotein E-coated LNP (ApoE-LNP) were considered under two different experimental configurations, with the LNP being either added to the somal or the synaptic compartment for anterograde or retrograde transport analyses, respectively. ApoE-LNP only were very efficiently uptaken by neurons and rapidly relocated in a perinuclear position. Also, ApoE-LNP incubated in the somal compartment did not translocate along the neurites (null anterograde transport), whereas ApoE-LNP added to the synaptic compartment were detected near the soma already at 30 min post incubation demonstrating retrograde transport velocities up to ~ 160 nm/s. This preliminary study suggests that ApoE-LNP could be efficiently used to rapidly transport a variety of therapeutic and imaging cargos from the synaptic cleft to the somal compartment.

1. Introduction

Neurons are cells with long axons and dendrites extending out from the cell body (soma) and regulating the transfer of information to and from the terminal synapses. Within the axons, molecules are transported via motor proteins, such as kinesin [1,2] and dynein [3–5], along the microtubules in the anterograde (soma to synapse) and retrograde (synapse to soma) directions. This process is fundamental to deliver newly synthesized substances, such as RNAs, proteins, organelles, and other materials, from the cell body to the axon terminals and collect aged materials back to the soma for degradation and recycling [1,6]. Dysfunction or failure of the axonal transport would inevitably impair a variety of neurological functions causing major deficits [7,8]. Notably, this same intracellular transport path is exploited by viruses that have been selected by nature to invade and efficiently infect the whole central nervous system (CNS). These neurotrophic viruses, such as the rabies, herpes simplex, varicella-zoster, west nile viruses and the poliovirus, have the ability to gain access to individual neurons from peripheral axons and translocate to the neuronal cell bodies spreading within the CNS via axonal transport [9–14]. Most of them are capable of both retrograde and anterograde transport. Interestingly, all these viruses have a characteristic size comparable with that of most nanomedicines. Specifically, the rabies virus [2] has a bullet shape with an overall length of ~200 nm and a cross section of ~100 nm; the herpes simplex [15] and varicella-zoster viruses [16] have an overall spherical shape with a diameter ranging between 150 and 250 nm, whereas the west nile virus [17] and poliovirus [18] have a much smaller diameter in the order of 50 nm. Inspired by this family of viruses, nanomedicines could be designed to exploit both retrograde and anterograde transport mechanisms and deliver bioactive molecules within the CNS [19–23], partially bypassing the otherwise impermeable blood-brain barrier (BBB) [24]. Nanoparticles (NP) can be designed to be uptaken by neurons via endocytosis [25], both at the axonal termini and cell body. When uptake occurs at the periphery, NP would be transported towards the neurons' body by retrograde transport in endocytic vesicles associated with dynein and accumulate in the soma [26]. In general, NP uptake and subsequent intra-neuronal transport could be facilitated by the surface conjugation of specific targeting moieties [27], such as the non-toxic fragments of the tetanus toxin, known as the tetanus toxin C fragment (TTC) [28]; and the apolipoprotein E (ApoE), the dominant lipoprotein

* Corresponding author.
E-mail address: roberto.palomba@iit.it (R. Palomba).

https://doi.org/10.1016/j.jddst.2024.106282
Received 14 March 2024; Received in revised form 8 October 2024; Accepted 10 October 2024
Available online 16 October 2024

in the brain [29]. Indeed, TTC-labeled NP were shown *in vitro* to bind to neurons with high specificity and affinity and undergo retrograde transport [28]. Also, intracranially administered ApoE-labed LNP were shown to enter neurons and successfully silence the expression of specific genes upon small interfering RNA (siRNA) delivery [29]. ApoE exposed on LNP allows for a superior uptake in neurons since nanoparticles are more prone to bind LDL receptor related protein 1 (LRP1) and low density lipoprotein receptor (LDLR), the two main ApoE receptors expressed on neuron plasma membrane [30].

Over the years, a large variety of microfluidic-based chips have been proposed to characterize axonal transport in neurons [31–38]. Particularly useful are the compartmentalized microfluidic chips presenting two chambers (somal and synaptic compartments) connected by multiple hundred micron-long channels. This chip design allows the fluidic isolation of the synaptic and somal compartment while guiding the growth and development of neuronal axons along the channels themselves. In these chips, the retrograde or anterograde transport properties of man-made and natural particles can be investigated by incubating them with the neurons on the synaptic or somal compartment, while fluidic isolation ensures that transport occurs along the axons rather than via passive diffusion within the culture media. Such microfluidic systems have been used for a variety of biophysical assays, including the labeling of neurons via a modified rabies virus [37], and the retrograde transport of gold [38] or polystyrene NP [36]. Considering the scientific and clinical relevance of lipid nanoparticles (LNP) for the cytosolic delivery of therapeutics, including nucleic acids [39], in our study naïve LNP and ApoE-LNP were first synthesized and characterized for their physico-chemical properties and toxicity profiles. ApoE-LNP were then tested for axonal transport in primary hippocampal neurons, grown in compartmentalized microfluidic chips, via live-cell fluorescent microscopy.

2. Materials and methods

Materials. 1,2-dipalmitoyl-sn-glycero-3-phosphocholine (DPPC), 1,2-dioleoyl-3-dimethylammonium-propane (DODAP), 1,2-distearoyl-sn-glycero-3-phosphoethanolamine-N-[methoxy(polyethylene glycol)-2000] (DSPE-PEG), 1,2-dipalmitoyl-sn-glycero-3-phosphoethanolamine-N-(lissamine rhodamine B sulfonyl) ammonium (Liss Rhod PE) were purchased from Avanti Polar Lipids Inc (Alabaster, AL). Cholesterol was purchased from Merck. Recombinant human apolipoprotein E3 (ApoE) was obtained by Peprotech (London, UK).

LNP preparation. The Nanoassemblr Benchtop (Precision NanoSystems, Vancouver, BC) was used to realize LNP, following standard protocols [40]. Briefly, a lipid mixture in ethanol (DODAP, DPPC, cholesterol, DSPE-PEG, Liss Rhod PE at 49.9/10/38.5/1.5/0.1 mol ratio) was rapidly mixed in the microfluidic chip with citrate buffer (pH 3.9, 50 mM) at a flow rate ratio (FRR) of 1:4 and a total flow rate (TFR) of 2 ml/min. The obtained LNP (1 ml) were dialyzed overnight (Pur--A-Lyzer Midi, 3.5 kDa MWCO) against PBS pH 7.4 (500 ml), then filter sterilized through 0.22 μm PVDF syringe filters (Millipore), and stored at 4 °C until use. Coating with ApoE was performed on the day of the experiment by mixing the preformed LNP with ApoE at a total lipid: protein ratio of 54:1 (w/w). ApoE was reconstituted following the vendor instruction to 1 mg/ml. The ApoE solution was gently pipetted in a tube containing the LNP and the mixture was incubated for 5 min at 37 °C to yield ApoE-LNP.

LNP characterization. The hydrodynamic diameter, polydispersity index (PdI), and surface ζ-potential of LNP and ApoE-LNP were measured using a Malvern Nano-ZS Zetasizer (Malvern, Worcestershire, UK), by diluting the samples 1:100 in deionized water. The morphology and internal structure of LNP was visualized by cryo-Electron microscopy (FEI Tecnai G2-F20). The amount of ApoE adsorbed on the surface of LNP was quantified by BCA (Euroclone), after dialyzing the ApoE-LNP against PBS for 24 h to remove the unbound ApoE (Float-A-Lyzer G2, 300 kDa MWCO).

Isolation and culture of primary hippocampal rat neurons. Pregnant rats (Sprague–Dawley, Charles River) were anesthetized and euthanized by inhalation of CO_2. 18-day embryos (E18) were removed immediately by cesarean section and sacrificed by decapitation. Brains were removed from the skulls and put in cold Hank's balanced salt solution (HBSS). The hemispheres were separated, and the meninges removed. The hippocampi were dissected out and incubated in trypsin-EDTA at 37° for 30 min. The resulting tissue was resuspended in Neurobasal Medium with 10 % FBS (Fetal Bovine Serum, gibco, Life Technologies), and centrifuged for 5 min at 1200 rpm to completely remove and replenish the medium with fresh one. The solution was resuspended and filtered to remove clumps and centrifuged for 7 min at 700 rpm to remove debris. Then, the medium was completely removed again. Finally, fresh Neurobasal Medium (without FBS) was added again to the pellet. Eventually, cells were counted and seeded at the desired concentration. Primary neurons were cultured with complete Neurobasal Medium (gibco, Life Technologies, REF. 21103–044) supplemented with 2 % B-27 (gibco, Life Technologies, REF. 17504–044), 1 % GlutaMAX (gibco, Life Technologies, REF35050-038), and 1 % Pen/Strep solution (Sigma-Aldrich, P4333) in 12-well plates or in compartmentalized microfluidic chips for 7 days to allow the axon/neurites growth prior to use in further experiments.

Neurons viability and particle uptake. Following the incubation of neurons with LNP or ApoE-LNP for 0.5, 1, and 2 h, the medium was removed, and the cells were washed with PBS and incubated with fresh Neurobasal Medium with 1 μM Calcein AM (Invitrogen, ThermoFisher, C1430). Live cells were detected and quantified based on their green intensity (Calcein AM positive, live cells). The intensity of the Calcein AM fluorescence was quantified by confocal microscopy (maximum projection) using the ImageJ software. Viability was quantified as the percentage of viable cells calculated from the fluorescence intensity of the Calcein AM signal under different experimental conditions. The LNP and ApoE-LNP uptake by neurons was assessed via flow cytometry. For this analysis, 80,000 cells were seeded into a 12-well plate and treated with LNP and ApoE-LNP at different time point. After the treatment, cells were washed with PBS, 200 μl of tripsin EDTA were added to each well, the culture was placed inside the incubator for 5 min, and the same volume of media was added. Then, cells from 3 different wells were resuspended in 200 μl of media, filtered by using a cell strainer (70 μm) and placed on ice and vortexed right before the analysis. Flow cytometry was performed using a FACS ARIA (Becton Dickinson, USA). The cell population was selected setting a scatter gate excluding the negligible number of debris and aggregates in the samples and taking into account the side scatter shift due to internal complexity changes caused by the internalized LNP. The population of cell positive for internalization was selected considering the basal level of fluorescence of the untreated cells.

Neuron metabolic activity – MTT assay. Cellular metabolism in 2D monolayers was evaluated using the MTT assay, following the supplier's instructions. Primary neurons were seeded into a 12-well plate and after 7 days incubated with LNP or ApoE-LNP for 0.5, 1, and 2 h. At the end of the treatment, cells were gently washed with PBS and incubated with MTT (0.25 mg/ml) for 3 h. Formazan crystals were dissolved in ethanol and the optical density (OD) was read at 490 nm. Cell viability was calculated as the difference in OD values obtained for the controls (untreated neurons) and the OD measured for the neurons exposed to LNP and ApoE-LNP, for all considered time points.

Compartmentalized microfluidic chips. Microfluidic devices with 150 μm long microchannels preassembled on optically transparent plastics (Xona microfluidics, XC150) were coated with 0.5 mg/ml poly-D-lysine hydrobromide (Sigma-Aldrich, P6407) at 37 °C overnight and subsequently washed with sterile deionized water. A suspension of primary neurons with cell density of 5 million/ml was prepared and 20 μl of the suspension were plated in the somal compartment of the microfluidic device. The axonal/neurite growth was guided by the microchannels from the somal towards the synaptic compartment. The

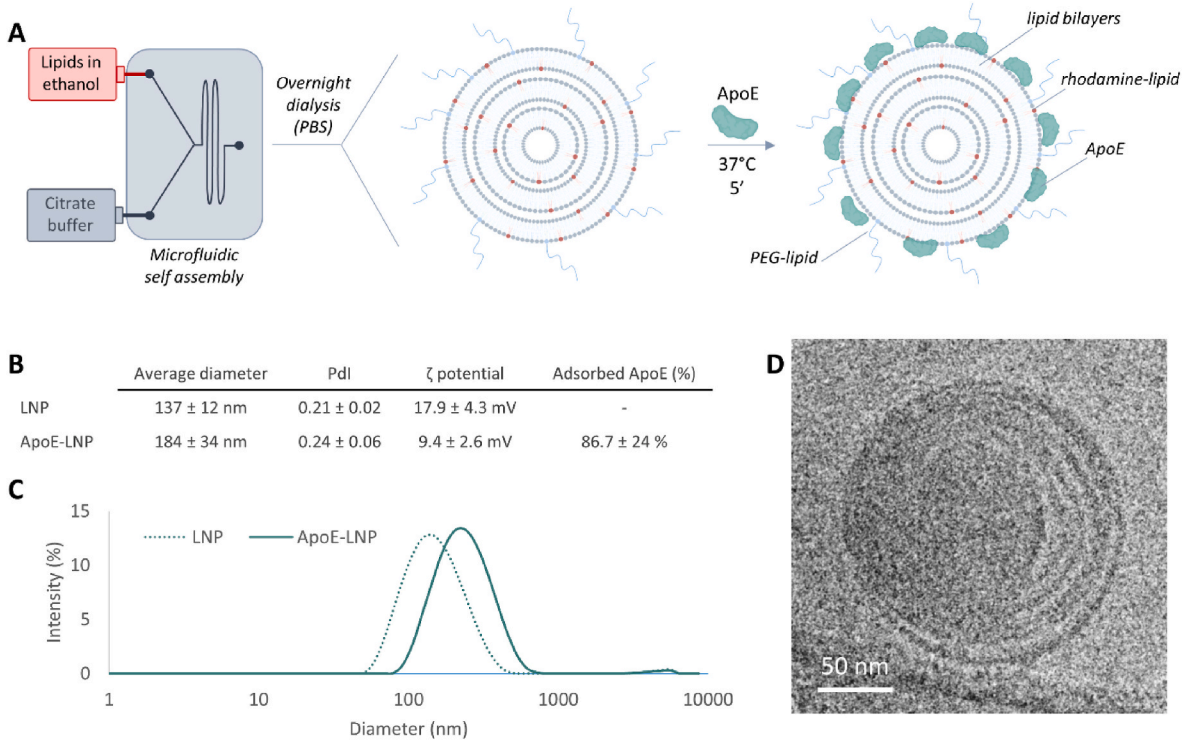

Fig. 1. Synthesis and Physico-chemical characterization of the Lipid Nanoparticles. A. Schematic representations of the microfluidic-based system for the production of LNP (***left***) and architecture of the LNP with lipid chains arranged in multilamellar vesicles containing red fluorescent Rhodamine-B molecules and the neuron targeting protein ApoE (***center*** and ***right***); **B**. Table listing the average hydrodynamic diameter, polydispersity index (PdI), and surface electrostatic ζ-potential derived from dynamic light scattering (DLS) analyses, and the percentage of ApoE adsorbed on the LNP surface; **C**. Size distribution of LNP and ApoE LNP as determined via DLS; **D**. Cryo-electron micrography of a LNP. (For interpretation of the references to color in this figure legend, the reader is referred to the Web version of this article.)

difference in volume of the solutions between the somal and synaptic compartment allowed for the fluidic isolation of the two compartments. The microchannels also prevented the passage of cell bodies. This allows one to study the axonal transport of NP both in the anterograde and retrograde directions. LNP or ApoE-LNP were exposed to neurons in the somal or synaptic compartments for 0.5, 1 and 2 h with the objective of quantitatively assess their axonal transport properties. After the predetermined incubation period, the excess of NP was washed away with fresh neurobasal medium. At least five microfluidic devices per condition were used and imaged at each time point, and for each channel.

Confocal fluorescence microscopy analysis. Confocal fluorescence microscopy (Nikon A1R+/A1+; objectives Nikon, 20× or 40×) was used to document the organization and viability of hippocampal neurons in 2D cultures and in the compartmentalized microfluidic chips as well as to localize the NP and track their axonal transport over time. Confocal fluorescence microscopy was also used to quantify LNP internalization into cells. After each predetermined time period (0.5, 1, and 2 h), z-stack sections were acquired using a 40× objective, and maximum intensity projection images were generated. Each experiment involved the acquisition of a minimum of eight images per condition and was repeated at least three times. High-resolution z-stack images were processed for 3D reconstruction and the fluorescence intensity was measured using the NIS-Elements AR (Nikon) software. NP were considered internalized by the neurons when their edges were fully included in the neurites or the cell body as from the lateral projection planes (x−z, z−y) and 3D surface reconstructions. Cell viability with no NP (control) at different time points was determined measuring the mean fluorescence intensity signal exhibited by Calcein AM. The relative position of NP and cell membranes was assessed in 2D or in the microfluidic devices to characterize the type of axonal transport.

Immunofluorescence. Primary neurons were fixed using 4 % paraformaldehyde in PBS at 37 °C for 20 min. Fixative was removed and cells were washed three times with PBS for 5 min. Subsequently, neurons were permeabilized with 0.1 % Triton X-100 for 30 min and blocked with 20× bovine serum albumin in PBS at room temperature for 30 min. Cells were then incubated with the primary antibody Anti-Beta III Tubulin (Invitrogen, ThermoFisher Scientifics, Cat. AB9354), (1:1000) overnight at 4 °C. In the following day, neurons were washed three times with PBS for 5 min and incubated with the Goat anti-Chicken IgY (H + L) secondary antibody (Alexa Fluor 488, Invitrogen, ThermoFisher Scientifics, Cat. A11039), (1:500) for 1 h. Finally, DAPI (Thermo Fisher Scientific) was added to neurons for 15 min, which were washed several times with PBS before confocal microscopy analysis. To compare the axonal and somatic uptake of LNP and ApoE-LNP, the normalized intensity of the fluorescent signal associated with the nanoparticles (fluorescence intensity × area) was measured.

Time-Lapse Microscopy Analysis. For time-lapse microscopy experiments, primary neurons seeded into the compartmentalized microfluidic device (Xona microfluidics, XC150) were observed as described above. A Nikon Eclipse-Ti-E microscope (Nikon Corporation, Japan) was used for this analysis. At day *in vitro* (DIV) 7, Rhodamine B-labeled ApoE-LNP were added to the chips for 2 h. After the treatment, the synaptic compartments of the chips were washed with complete neurobasal medium to remove most of the free or loosely attached particles (not firmly bound to neurons). Time-lapse movies were acquired in bright-field and tetramethylrhodamine (TRITC) channels, until 4 h post chip washing. During the acquisitions, cells were kept in controlled environmental conditions at 37 °C in a humidified 5 % CO_2 atmosphere in complete neurobasal medium. Movies were acquired at 1 or 2 frames per minute (depending on the number of the field imaged in the chip per experiment). The acquisition was performed on four chips, considering from 4 to 10 different regions of interest per chip, where each chip

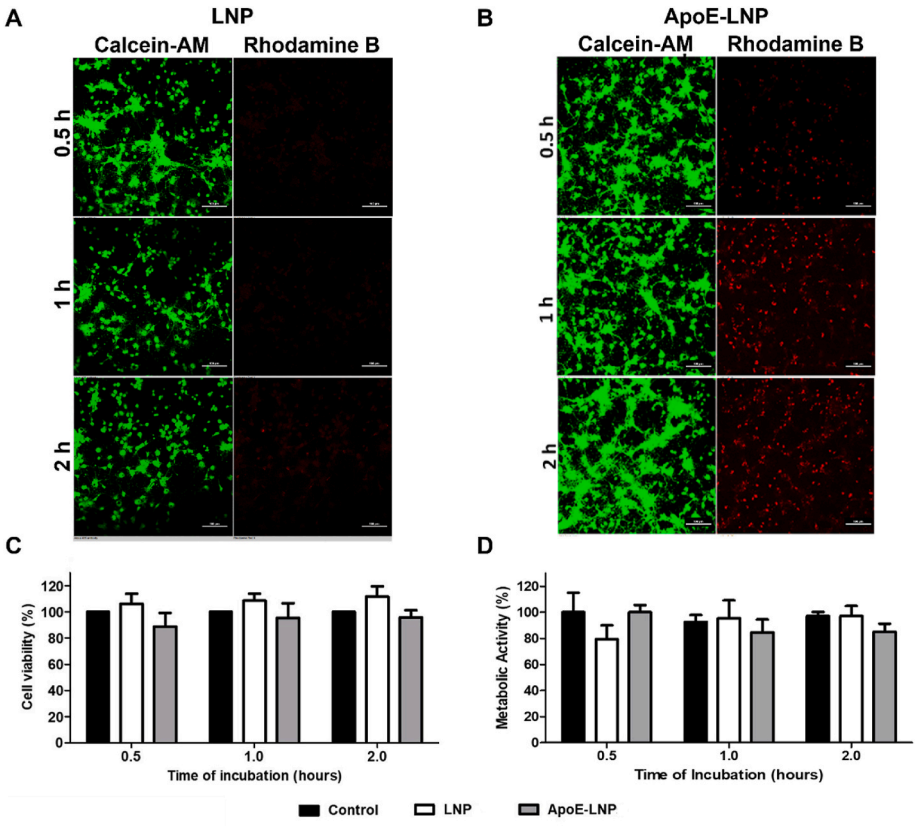

Fig. 2. Toxicity profiles of the Lipid Nanoparticles. A. and **B**. Representative confocal microscopy images (maximum intensity projections) for Calcein-AM (***left***) and Rhodamine-B (***right***) of primary hippocampal neurons incubated with naïve LNP **(A)** and ApoE-LNP **(B)** for 0.5, 1, and 2 h. Viable cells (***green***), LNP (***red***); **C.** Cell viability measured from maximum intensity projections confocal microscopy images stained with Calcein-AM; **D.** Metabolic activity of neurons via MTT assay. Scale bar corresponds to 100 μm and applies to all images. (For interpretation of the references to color in this figure legend, the reader is referred to the Web version of this article.)

represented one biological replicate. A projection of the LNP position over time was generated on the x-axis, considering the particle as a moving point on a Cartesian plot. Sections of the microchannel where LNP were observed to move were cropped and a superimposition of all the frames (4 h) of the TRITC channel was generated to reconstruct the particle trajectory. The velocity was calculated considering the cumulative displacement from the start to the end points.

Confocal imaging of a single microchannel. Following the same procedure for the seeding and LNP incubation with the neurons, a subset of microfluidic chips was fixed and stained for actin and cell membranes. For this specific staining, a mixture of Alexa Fluor-488 Phalloidin, Alexa Fluor-647 Wheat Germ Agglutinin, and DAPI was added according to vendors dilution for 40 h at 4 °C. Confocal images of axons inside the microchannels were obtained using a Nikon-A1 confocal microscope (Nikon Corporation, Japan) and a 60× objective. The 3D reconstruction of the axon was performed by using Nikon Imaging Software.

Statistical analysis. Data are expressed as mean ± standard deviation using GraphPad Prism 5 software. Calculation of cell viability, metabolic activity, and NP internalization were analyzed via ANOVA.

3. Results and discussion

Synthesis and biophysical characterization of the lipid nanoparticles. Rapid microfluidic mixing of lipids dissolved in ethanol with a citrate buffer allowed the production of lipid nanoparticles (LNP), as per the schematic in Fig. 1A. For this study, LNP were prepared without RNA cargos and contained only a Rhodamine B-tagged lipid, amenable for fluorescent tracking. Dynamic light scattering measurements, performed after dialysis and sterile filtration, returned for the LNP an average hydrodynamic diameter of ~150 nm with a narrow polydispersity index (PdI) (Fig. 1B). As shown by others, incubation at 37 °C did not affect their average diameter of LNPs [41] and they are stable upon incubation in cell culture medium [42]. Coating the LNP with the targeting protein ApoE, via surface absorption, led to an increase in particle size from the native 137 ± 12 to 184 ± 34 nm (Fig. 1B and **C**). The LNP morphological examination by cryo-Electron microscopy confirmed the arrangement of the lipid chains into multilamellar vesicles (Fig. 1D). Due to the overall negative charge of ApoE, LNP coating resulted in a reduction of the native positive charge with a ζ-potential decreasing from +17.9 ± 4.3 to +9.4 ± 2.6 mV (Fig. 1B). Most of the ApoE molecules incubated with the LNP firmly adsorbed on the particle surface, as up to ~90 % of the protein was recovered from ApoE-LNP at 24 h post dialysis against PBS (Fig. 1B).

In order to test the LNP biocompatibility, the viability of primary neurons incubated with the LNP was assessed at predetermined time points. Rat primary hippocampal neurons were cultured in 2D and incubated with naïve LNP or ApoE-LNP (Fig. 2A and **B**). Calcein AM staining of the primary neurons revealed no difference in viability, morphology, or organization of the cells when comparing the LNP exposed cells to the untreated cells (control experiments - no incubation with LNP). In Supporting Fig. 1A and **B**, we report higher magnification images showing the merging between the green channel (Calcein-AM associated with the neurons) and the red channel (RhB associated with the LNP) after 2 h of incubation with LNP or ApoE-LNP, respectively. These images clearly show a preferential uptake of the ApoE-LNP over the naïve LNP, which after 2 h were poorly uptaken by the neurons. Quantitative cell viability values were extracted from these images as documented in bar chart of Fig. 2C. No statistically significant changes

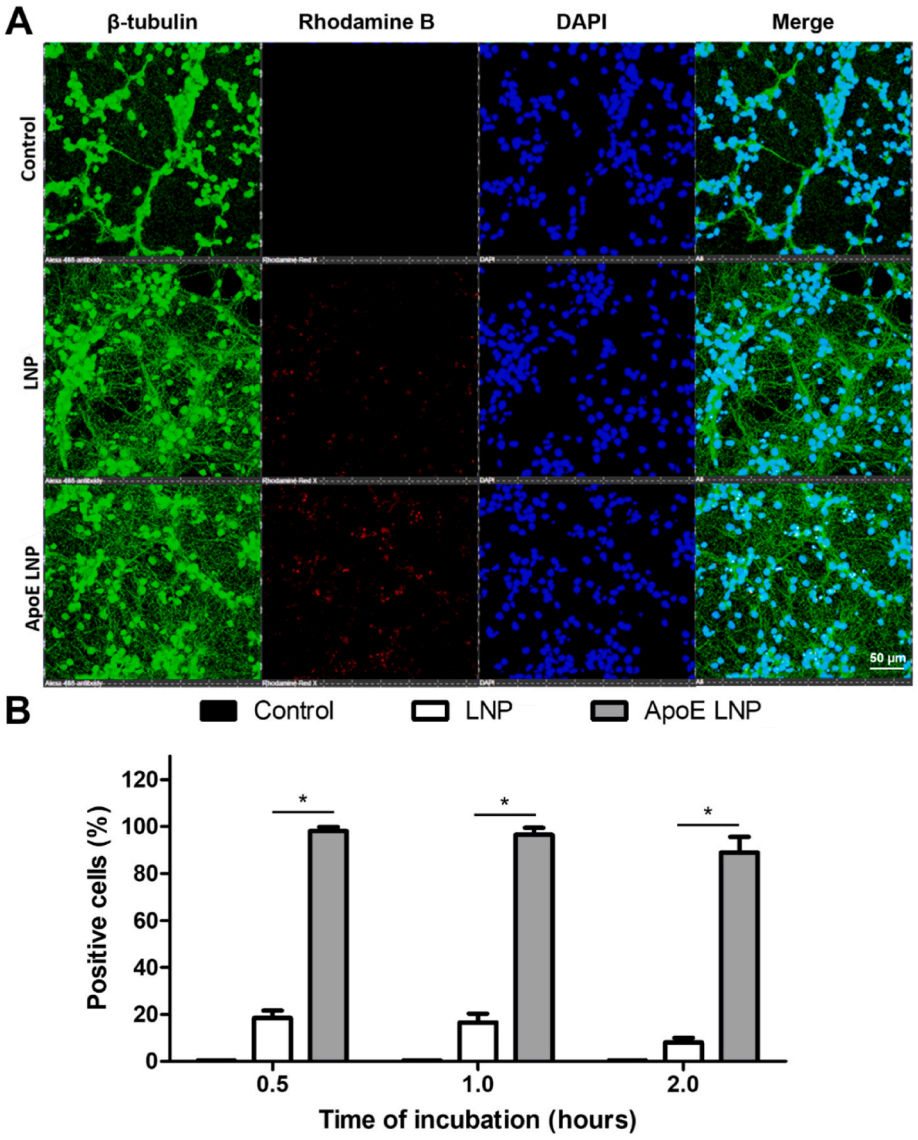

Fig. 3. Internalization of Lipid Nanoparticles into 2D neuron monolayers. A. Representative maximum intensity projections of immunofluorescence confocal microscopy images of neurons incubated with naïve LNP, ApoE-LNP, and without LNP (control). Nuclei in blue (DAPI), neurites in green (β-tubulin staining), LNP in red (Rhodamine-B); **B.** Quantitative measurement of LNP uptake as a function of the incubation time by flow cytometry. (*) $p < 0.01$ significant difference between LNP and ApoE-LNP at different time points. (For interpretation of the references to color in this figure legend, the reader is referred to the Web version of this article.)

were observed for all the tested conditions and at all predetermined time points, as compared to the control experiments. To further support this data, we performed an MTT assay to quantify the metabolic activity of primary neurons after the exposure to LNP (Fig. 2D). No evidence of any cytotoxic activity was documented even in this case up to 2 h, with the metabolic activity of the particle-free neurons being statistically identical to that of cells exposed to LNP or ApoE-LNP. As expected, these LNP and ApoE-LNP do not exert any deleterious effect on primary neurons within the predetermined observation period.

Uptake of the lipid nanoparticle by neurons. ApoE-LNP and LNP were incubated with hippocampal neurons (on day 7 after seeding) at different predetermined times, namely 0.5, 1 and 2 h. Cells were cultured following the same conditions used for viability experiments. Fig. 3A gives fluorescent confocal microscopy images for the control cells (top row), cells exposed to RhB-LNP (central row), and cells exposed to RhB-labeled ApoE-LNP (bottom row). The first column (green channel) gives the tubulin staining identifying the body of the neurons; the second column (red channel) refers to the Rhodamine-B labeled nanoparticles; the third column (blue channel) derives from the nuclei of the cells stained with DAPI; and the fourth column provides the merging of the three channels. The Rhodamine-B signal shows that ApoE-LNP were more abundantly internalized as compared to LNP within the same time. The more abundant and rapid uptake of the ApoE-LNP over the naïve LNP was confirmed by quantitative measurements performed by flow cytometry. Here, 98.1 ± 1.7 % of the neurons were found to be associated with ApoE-LNP already after 30 min as opposed to a modest 20 % in the case of the naïve LNP, at the same incubation time (Fig. 3B).

To further support these findings, we coupled the flow cytometry data with high magnification confocal imaging analyses. Primary neurons on day 7 were fixed and immunostained with anti-β-tubulin III (green), while nuclei were stained with DAPI (blue) (Fig. 4A). In this case too, neurons were exposed to LNP or ApoE-LNP for 0.5, 1, and 2 h. High magnification images (Fig. 4A–C) show that most ApoE-LNP were localized in a perinuclear zone rather than within the neurites, and the lateral projections show the red fluorescence associated with the nanoparticles encased within the green fluorescence delineating the cell body. The higher internalization rate of ApoE-LNP compared to LNP is

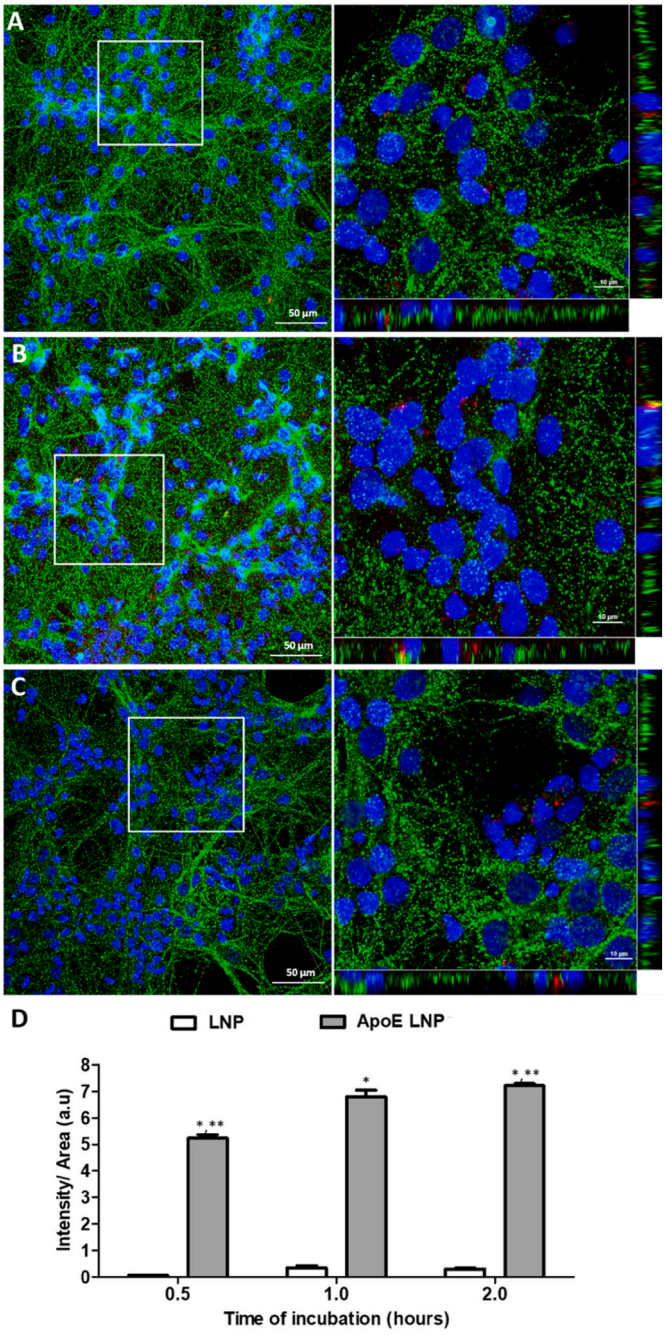

Fig. 4. Internalization of ApoE-LNP into 2D neuron monolayers. A-C. Representative maximum intensity projections of immunofluorescence confocal microscopy images of hippocampal neurons after 0.5 h (**A**), 1 h **(B)**, and 2 h **(C)** incubation with ApoE-LNP, documenting the accumulation of ApoE-LNP around the nuclei; **D.** Quantitative internalization of LNP over time. β-tubulin-positive neurons (green), nuclei were counterstained with DAPI (blue), ApoE-LNP stained with Rhodamine-B (red). (*) $p < 0.01$ significant difference of internalization of ApoE-LNP at different time points; (**) $p < 0.05$ significant difference between internalization of LNP and ApoE-LNP at the same time point. (For interpretation of the references to color in this figure legend, the reader is referred to the Web version of this article.)

also evident in this confocal microscopy analysis, as naïve-LNP cannot be easily detected in neurons at the different time points (Supporting Fig. 2). Quantitative intensity measurements (Fig. 4D) indicate a clear and significant uptake of ApoE-LNP vs LNP. As expected from the previous test, after only 0.5 h, ApoE-LNP were detected within neurons (Fig. 4A); LNP were instead almost undetectable even 2 h post-incubation (Supporting Fig. 2). The quantification of particle internalization at 0.5 h, expressed by fluorescent intensity (red signal) per unit cell area, returned the values 5.24 ± 0.32 a.u. vs 0.07 ± 0.02 a.u. for ApoE-LNP and naïve-LNP, respectively (Fig. 4D). At the longer time points, after 1 and 2 h, data continued to show a significant advantage for the ApoE-LNP over the LNP: 6.80 ± 0.55 vs 0.35 ± 0.19 a.u. and 7.22 ± 0.16 vs 0.31 ± 0.07 a.u, respectively (Fig. 4D). Cumulatively, these data support the observation that ApoE coating facilitates the neuronal uptake of LNP, which would be otherwise very minimal at the considered time points. Not only the number of positive cells resulted higher (flow cytometry measurements), but also the intensity per area parameter was larger in ApoE-modified when comparing to naïve LNP.

Axonal transport of the lipid nanoparticles. To study the retrograde and anterograde translocation of the nanoparticles, a compartmentalized microfluidic chip was used to ensure that the soma and axonal terminations of the neurons were kept always separated. Fig. 5A shows on the left a schematic of the chip where the somal compartment (**a** – blue area) is fluidically isolated from the synaptic compartment (**c** – yellow area) and connected only via 150 μm long microchannels (**b**), within which axons grow and develop over time. In order to verify the isolation between the two compartments, two different fluids were added in a test chip, namely a black fluid on the somal compartment and a red fluid on the synaptic compartment (Fig. 5A – **right inset**). After cell seeding and growth, the presence of fully developed axons within the microchannels ensures the fluidic isolation of the two compartments, as documented by the lack of mixing of the black and red fluids. A schematic of a neuron is proposed at the bottom.

For the transport experiments, hippocampal neurons were seeded in one of the two compartments, and after 7 days of culture, axons were observed to extend within the microchannels (Fig. 5B). Anterograde transport was first tested: cells were treated by adding Apo-E LNP or LNP to the somal compartment for 0.5, 1, and 2 h. In this configuration Apo-E LNP rapidly accumulated in the perinuclear area of the neurons and did not translocate to the axon compartment, as shown in Supporting Fig. 3. When using instead naïve LNP, no particles were observed to accumulate in the perinuclear area (Supporting Fig. 4A), confirming to the poor cell uptake observed in previous experiments.

Retrograde transport was then tested, again with both particles and respecting the same time points. When adding ApoE-LNP to the synaptic compartment, they were rapidly uptaken and transported along the microchannels within the axons towards the somal compartment as shown in Fig. 6. When using LNP under the same configuration we were able to visualize only few particles in the axonal compartment, as shown in Supporting Fig. 4, and no particle in the somal compartment. These observations would suggest that ApoE functionalization is capable of increasing LNP uptake, and to grant them a fast translocation from the axonal to the somal compartment. Due to the limited internalization of the naïve LNP, and to the fact that no anterograde transport was found for both particles, the following specific translocation analyses were only performed on Apo-E LNP.

For characterizing Apo-E LNP transport, we divided the acquired images of the microfluidic chips in three region of interest (ROI) – (a) soma, (b) microchannels, and (c) synaptic side – and the fluorescence intensity of ApoE-LNP was measured in each ROI at different time points. Representative fluorescent images of the somal and synaptic compartments together with the microchannels are shown in Fig. 6A–C for different incubation times, namely 0.5, 1 and 2 h. The bar chart of Fig. 6D reports the intensity of the fluorescent signal in each specific section – soma, microchannel, synaptic – at the different time points, normalized by the total intensity measured within the overall area. After 0.5 h, ApoE-LNP were detected into the microchannels (42.2 % ± 3.8 %) at significantly higher rates than in the synaptic (29.2 % ± 3.6 %) and somal (26.4 % ± 3.0 %) compartments (Fig. 6A–D). This would imply that after only 0.5 h, ApoE-LNP were internalized by the synapses and translocated to the soma through the 150 μm long microchannels. After 1 h, most of the ApoE-LNP were again detected inside the microchannels

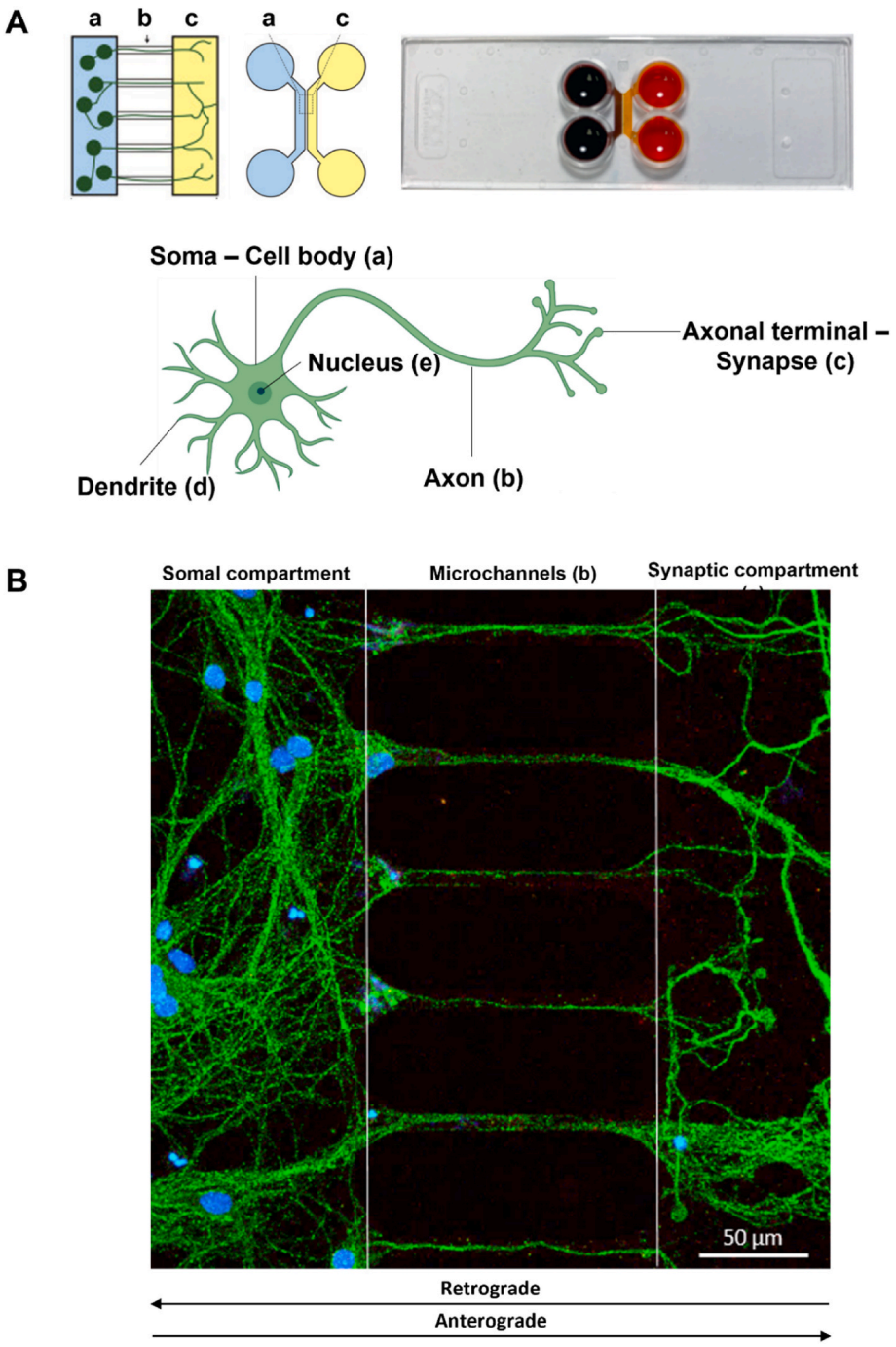

Fig. 5. Compartmentalized microfluidic chip for LNP axonal transport studies. **A-*left***. Microfluidic chip showing the somal compartment **(a)**, the 150 µm long microchannels **(b)**, and the axonal compartment **(c)**. The lower image shows the structure and components of a neuron; **A-*right*.** Microfluidic chip filled with two different liquids demonstrating the separation between the solution in the somal compartment (black) and the synaptic compartment (red) – fluidic isolation; **B**. Representative maximum projection confocal image of primary hippocampal neurons cultured for 7 days into the microfluidic chip showing the β-tubulin III labeled neurites (green) extending from the somal compartment to the synaptic compartment through the 150 µm microchannels. (For interpretation of the references to color in this figure legend, the reader is referred to the Web version of this article.)

(50.5 ± 4.7 %) and at the soma compartment (Fig. 6B), in a perinuclear position (Fig. 6B – high magnification). After 2 h, there was a significant accumulation of ApoE-LNP in the final part of the microchannels towards the soma and in the soma itself (38.7 % ± 3.2 %) (Fig. 6C).

Retrograde transport of the ApoE-coated lipid nanoparticles. The transport dynamics of ApoE-LNP were also investigated by time-lapse microscopy for defining particle displacement and velocity within the axons of hippocampal neurons. Herein, Rhodamine-B labeled ApoE-LNP were individually tracked to determine trajectories and average velocities. Hippocampal neurons were seeded in the microfluidic chip as indicated above and ApoE-LNP were incubated in the synaptic compartment for 2 h. After that, the compartment was washed twice with fresh complete neurobasal medium to remove loosely bound and not-internalized LNP. Time-lapse movies were acquired in bright-field and TRITC channels, up to 4 h post incubation. In Fig. 7A we show a representative image of the chip (left) and on overlap all the movie frames as maximum intensity projection (right). The regions in the microchannels where ApoE-LNP were observed to move were

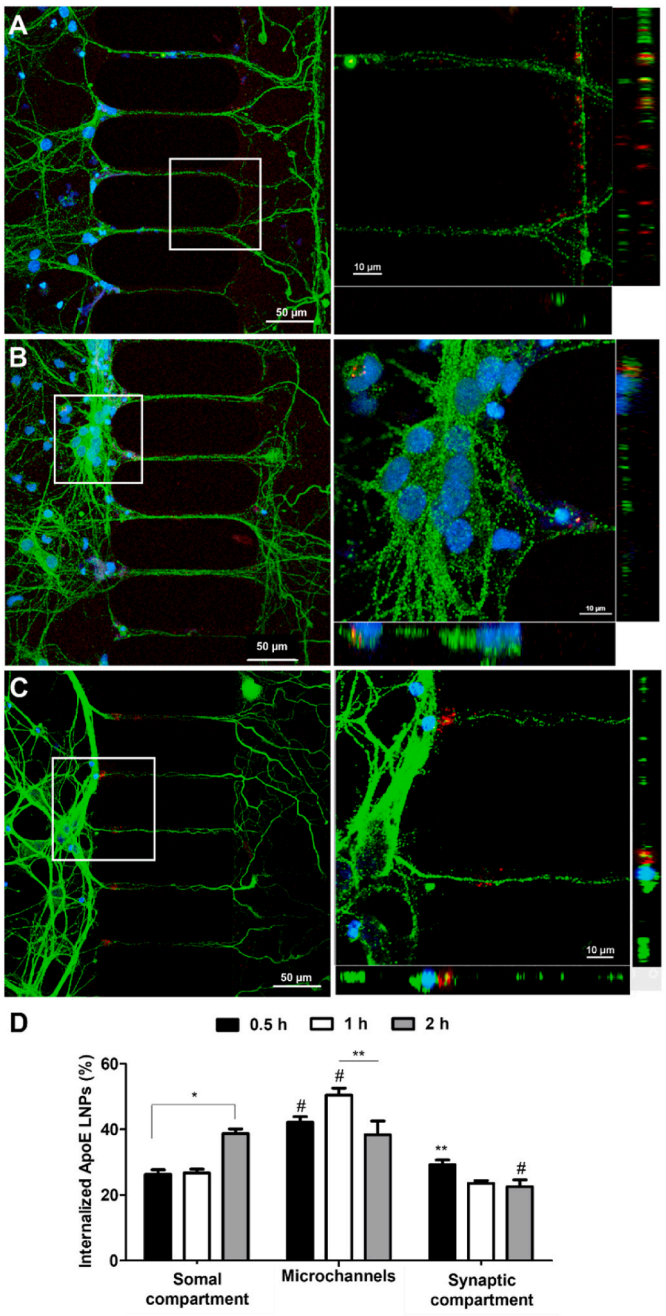

Fig. 6. Localization of ApoE-LNP into the compartmentalized microfluidic chip (LNP incubation in the synaptic compartment). A-C. Representative maximum intensity projections of immunofluorescence confocal microscopy images of neurons cultured into microfluidic chips on day 7 and incubated with ApoE-LNP for 0.5 h **(A)**, 1 h **(B)**, and 2 h **(C)**. The images show the internalization of ApoE-LNP in the synaptic compartment at the early time points (red dots in **A**) and their transport towards the soma and preferential perinuclear accumulation at the latest time points (red dots in **B** and **C**); **D.** Measurement of ApoE-LNP internalization and their localization over time. (#) $p < 0.01$ localization of nanoparticles at the same time point; (*) $p < 0.01$, (**) $p < 0.05$ localization of nanoparticles at different time points. (For interpretation of the references to color in this figure legend, the reader is referred to the Web version of this article.)

identified, and ApoE-LNP displacements were reconstructed over time, as shown in the representative image proposed in Fig. 7B (top). The yellow line and the circles in Fig. 7B (bottom) were used to highlight particle trajectory. The average velocity was calculated as the cumulative displacement from the starting point (S) to the final point (F) divided by the observation time. In terms of particle velocity, our analysis registered a bimodal distribution, with ~67 % of the analyzed ApoE-LNP returning a speed of 164 ± 35 nm/s, and the remaining 33 % of ApoE-LNP moving at a considerably lower speed of 0.95 ± 0.42 nm/s (Fig. 7C). At the end of the analysis, neurons were fixed and immunestained for β-tubulin (green signal), Alexa-fluor-647-WGA for the cell membrane (red signal), while Apo-E LNP were false colored in white. Neurons were imaged at the confocal microscope for visualizing the ApoE-LNP position inside the axon. As it is shown in Fig. 7D, a considerable amount of ApoE-LNP was present at 4 h post-incubation, in agreement with the quantitative data of Fig. 6D. As shown by others, the axonal transport velocity of vesicles, organelles, proteins, nanoparticles, or other materials varies greatly. Specifically, it has been shown that organelles can be pushed out of the cell body at the considerable speed of 1 μm/s (400 mm/day) while proteins appear to be slower: <0.1 μm/s (<8 mm/day). Other endogenous compounds, as newly synthesized cytosolic proteins and cytoskeletal polymers, fall in two different categories, namely the 'slow component a' with translocation speeds ranging between 2.3 and 11.6 nm/s (0.2 and 1 mm/day) and 'slow component b' returning speed values between 11.6 and 116 nm/s (1 and 10 mm/day) [43]. As for endogenous vesicles, Cui et al. measured the speed of the retrograde transport of nerve growth factor (NGF)-containing endosomes revealing velocities ranging from 0.2 to 3 μm/s [21]. Similar values were also retrieved by Chowdary et al. when measuring retrograde transport of endosomes ([21,22]. Regarding nanoparticles, Lopes et al. measured the velocity of ~275 nm thiolated trimethyl chitosan-based particles to be ranging between 0.1 and 3 μm/s [34]. In another study, Nakamura et al. measured the velocity of CM-Dil Labeled particles (ranging from 0.93 to 1.86 μm in diameter size) revealing velocities ranging from 48 nm/s to 8 μm/s [44]; considering these information, axonal transport appear a multifactorial process depending on the unique physical and chemical features of the carrier, such as the size, surface charge, material, and other physiological/pathological parameters, such as the functionality of the molecular motors devoted to these processes [45]. On this last point, it is important to consider the effect of concurrent drug treatments on the function of molecular motors, as it was demonstrated that several drugs (e.g. vincristine, paclitaxel) can slow down axonal transport [44]. In the case LNP, Apo-E functionalization determined a considerable difference in terms of cellular uptake with respect to uncoated LNP, and particles returned a retrograde transport velocity of 164 ± 35 nm/s or 0.95 ± 0.42 nm/s. These values would suggest that ApoE-LNPs are retrogradely transported with slower velocities compared to endocytic vesicles, which could be directly compared in size to LNPs. From a drug delivery perspective, a desirable transport velocity for a CNS-targeted nanocarrier is not set yet, but fulfilling all the safety and efficacy requirements recommended for nanomedicines is strictly needed. With the regulatory approval of Onpattro (Alnylam), Comirnaty (Pfizer) and Spikevax (Moderna), LNPs have proven to be fit for purpose of safely delivering short interfering RNA and messenger RNA, respectively. Further studies on the efficacy of LNP treatment in CNS are needed, and the exploration of different compositions for enhancing axonal transport velocity might also broaden the application of LNP to CNS disorders.

3.1. ApoE-LNP potential applications for the treatment of diseases related to CNS

Following the COVID-19 pandemic, subcutaneous administration of LNPs for mRNA-based vaccines has become an established clinical practice. Similarly, one product based on intravenous LNPs received marketing authorization in 2018 [46], and several clinical trials are currently ongoing [47]. Regarding diseases of the CNS, local and systemic routes of administration are generally not completely suitable for neuronal delivery. The local route is limited by the invasiveness of the procedures when applied in brain settings, while the intravenous route faces challenges due to the blood-brain barrier (BBB). To enhance the

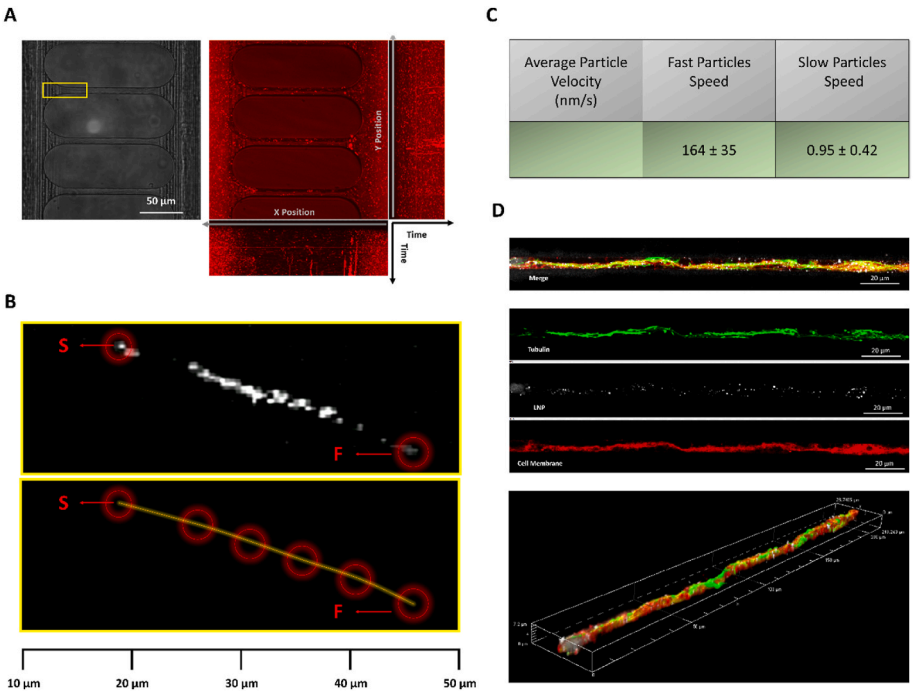

Fig. 7. Quantitative analysis of ApoE-LNP transport dynamics. **A**. Bright field image of the chip and a superimposition of all the frames over 4 h time lapse movie presented as maximum intensity projection of the red channel (ApoE-LNP in red); the yellow frame highlights a representative region of interest where particle motion was revealed and analyzed. **B**. One single ApoE-LNP trajectory (top) and its displacement over the time of 4 h (bottom); the starting (S) and the final (F) of the motion are indicated by an arrow. **C.** Particles velocity tab. **D**. Confocal fluorescent microscopy analysis of one micro-channel; from top to bottom: merge, green: α-tubulin, white: ApoE-LNP, red: cell membrane and 3D. (For interpretation of the references to color in this figure legend, the reader is referred to the Web version of this article.)

biodistribution of nanoparticles to the CNS, an increasing number of publications propose the nose-to-brain route for treating various neurological disorders. This route leverages the olfactory neurons, which extend from the olfactory epithelium in the nasal cavity (outside the CNS) to the olfactory bulb within the CNS, forming a privileged pathway [48].

For example, the nose-to-brain route has been used to promote brain accumulation of letrozole-loaded nano-emulsions and PLGA nanoparticles encapsulating diazepam for managing status epilepticus [49,50]. Other studies have targeted Alzheimer's disease by delivering liposomal donepezil or galantamine hydrobromide via the nose-to-brain route [51,52]. Many more examples are available in the review by Lee et al. [53]. The results reported in our study, highlighting the neuronal retrograde transport of ApoE-LNPs, strongly suggest that these nanoparticles could be efficiently employed for brain delivery via the nose-to-brain route.

ApoE-LNPs can also be designed to carry nucleic acid cargoes. With this in mind, the clinical applications of ApoE-LNPs may expand to pathologies stemming from genetic defects or altered processes that could benefit from nucleic acid-based treatments. ApoE-LNPs could serve as vectors for transfecting neurons with DNA, mRNA, siRNA, and other nucleic acids via the nose-to-brain route. Numerous nucleic-acid-based agents, delivered by the clinically approved LNPs, show promise for managing Alzheimer's disease [54], but these specific ones were not tested via the nose-to-brain route. It is the authors' opinion that adopting this route could significantly improve their therapeutic outcomes.

When using the nose-to-brain route, higher particle efficiency in entering cells and being transported by them reduces the required dose. Efficient transport is critical in designing particles with low toxicity, especially for neurons, whose delicate homeostasis can be easily disrupted. Our findings support the idea that ApoE functionalization of LNPs could represent a simple and effective strategy to improve neuronal delivery performance without altering the toxicity profile. Despite the superior uptake of ApoE-LNPs in neurons, cell viability and metabolic activity did not show significant changes. This, combined with the observation of retrograde transport, encourages further preclinical experimentation in specific models of neurological diseases, leveraging the nose-to-brain route. Given the versatility of LNPs, they could be loaded with drugs of varying chemistries (from nucleic acids to small molecules) and therapeutic mechanisms, thereby promoting their accumulation in the CNS and expanding the options for treating neurological diseases.

4. Conclusions

Herein, we investigate the axonal transport of Rhodamine-B labeled LNP in hippocampal primary neurons dynamically cultured in compartmentalized microfluidic chips using confocal fluorescence microscopy and live-cell time-lapse microscopy. LNP were either coated with the targeting protein ApoE or uncoated (naïve) and were incubated with the soma or synaptic termini of the neurons to assess the efficiency of anterograde versus retrograde transport, respectively. Uptake studies into primary neurons demonstrated that ApoE coating is crucial to favor LNP internalization. Different assays conducted on the primary neurons documented a fast ApoE-LNP internalization, occurring as early as at 0.5-h post incubation. Furthermore, when directly exposed to the synaptic termini, the ApoE-LNP were quickly uptaken and transported from the original site to the soma compartment along neurites in the 150 µm microchannels, reaching the soma within 0.5 h. On the contrary, when delivered in the somal compartment, ApoE-LNP were found around the nuclei and circumscribed to this compartment. The preferential retrograde transport of ApoE-LNP from the axon termini to the soma, analyzed by live-cell imaging, revealed transport velocities up to ~160 nm/s. In conclusion, the fast internalization and the retrograde transport of ApoE-LNP could be exploited to efficiently deliver biological cargos

from the periphery to the central nervous system. Considering the summarized features of ApoE-LNP and the versatility of their payloads, they could represent a powerful tool against several CNS diseases to be administered by nose-to-brain route.

CRediT authorship contribution statement

Ana M. Martins: Writing – original draft, Validation, Project administration, Investigation, Formal analysis, Data curation, Conceptualization. **Roberto Palomba:** Writing – review & editing, Writing – original draft, Visualization, Software, Methodology, Investigation, Conceptualization. **Michele Schlich:** Writing – review & editing, Writing – original draft, Visualization, Validation, Methodology, Investigation, Data curation, Conceptualization. **Paolo Decuzzi:** Writing – review & editing, Writing – original draft, Visualization, Validation, Supervision, Project administration, Funding acquisition, Conceptualization.

Declaration of competing interest

The authors declare that they have no known competing financial interests or personal relationships that could have appeared to influence the work reported in this paper.

Acknowledgments

This project was partially supported by the European Union's Horizon 2020 Research and Innovation Programme under the Marie Sklodowska-Curie grant agreement no. 754490 – MINDED. The authors gratefully acknowledge Marina Nanni at the Italian Institute of Technology for her help with the isolation of hippocampal neurons from rats and. The authors acknowledge the support provided by the Electron Microscopy Facility and the Nikon Imaging Center at IIT.

Appendix A. Supplementary data

Supplementary data to this article can be found online at https://doi.org/10.1016/j.jddst.2024.106282.

Data availability

Data will be made available on request.

References

[1] M. Terenzio, G. Schiavo, M. Fainzilber, Compartmentalized signaling in neurons: from cell biology to neuroscience, Neuron 96 (3) (2017) 667–679.
[2] A.R. Fooks, F. Cliquet, S. Finke, C. Freuling, T. Hemachudha, R.S. Mani, et al., Rabies, Nat. Rev. Dis. Prim. 3 (1) (2017) 17091.
[3] R.B. Vallee, J.C. Williams, D. Varma, L.E. Barnhart, Dynein: an ancient motor protein involved in multiple modes of transport, J. Neurobiol. 58 (2) (2004) 189–200.
[4] L.S. Goldstein, Z. Yang, Microtubule-based transport systems in neurons: the roles of kinesins and dyneins, Annu. Rev. Neurosci. 23 (1) (2000) 39–71.
[5] S.L. Reck-Peterson, W.B. Redwine, R.D. Vale, A.P. Carter, The cytoplasmic dynein transport machinery and its many cargoes, Nat. Rev. Mol. Cell Biol. 19 (6) (2018) 382–398.
[6] W.M. Saxton, P.J. Hollenbeck, The axonal transport of mitochondria, J. Cell Sci. 125 (Pt 9) (2012) 2095–2104.
[7] J.N. Sleigh, A.M. Rossor, A.D. Fellows, A.P. Tosolini, G. Schiavo, Axonal transport and neurological disease, Nat. Rev. Neurol. 15 (12) (2019) 691–703.
[8] S. Millecamps, J.-P. Julien, Axonal transport deficits and neurodegenerative diseases, Nat. Rev. Neurosci. 14 (3) (2013) 161–176.
[9] D.E. Griffin, Immune responses to RNA-virus infections of the CNS, Nat. Rev. Immunol. 3 (6) (2003) 493–502.
[10] H. Jang, D. Boltz, K. Sturm-Ramirez, K.R. Shepherd, Y. Jiao, R. Webster, et al., Highly pathogenic H5N1 influenza virus can enter the central nervous system and induce neuroinflammation and neurodegeneration, Proc. Natl. Acad. Sci. USA 106 (33) (2009) 14063–14068.
[11] S. Gluska, E.E. Zahavi, M. Chein, T. Gradus, A. Bauer, S. Finke, et al., Rabies virus hijacks and accelerates the p75NTR retrograde axonal transport machinery, PLoS Pathog. 10 (8) (2014) e1004348.
[12] D.G.R. Tervo, B.-Y. Hwang, S. Viswanathan, T. Gaj, M. Lavzin, K.D. Ritola, et al., A designer AAV variant permits efficient retrograde access to projection neurons, Neuron 92 (2) (2016) 372–382.
[13] S.E. Antinone, G.A. Smith, Retrograde axon transport of herpes simplex virus and pseudorabies virus: a live-cell comparative analysis, J. Virol. 84 (3) (2010) 1504–1512.
[14] S. Grigoryan, P.R. Kinchington, I.H. Yang, A. Selariu, H. Zhu, M. Yee, et al., Retrograde axonal transport of VZV: kinetic studies in hESC-derived neurons, J. Neurovirol. 18 (6) (2012) 462–470.
[15] R.F. Laine, A. Albecka, S. Van De Linde, E.J. Rees, C.M. Crump, C.F. Kaminski, Structural analysis of herpes simplex virus by optical super-resolution imaging, Nat. Commun. 6 (1) (2015) 1–10.
[16] J. Sun, C. Liu, R. Peng, F.-K. Zhang, Z. Tong, S. Liu, et al., Cryo-EM structure of the varicella-zoster virus A-capsid, Nat. Commun. 11 (1) (2020) 1–11.
[17] S. Kobayashi, C. Kaneko, R. Kawakami, R. Hasebe, H. Sawa, K. Yoshii, et al., Amino acid 159 of the envelope protein affects viral replication and T-cell infiltration by West Nile virus in intracranial infection, Sci. Rep. 10 (1) (2020) 1–9.
[18] M.W. Bahar, C. Porta, H. Fox, A.J. Macadam, E.E. Fry, D.I. Stuart, Mammalian expression of virus-like particles as a proof of principle for next generation polio vaccines, npj Vaccines 6 (1) (2021) 1–11.
[19] K. Sung, M.T. Maloney, J. Yang, C. Wu, A novel method for producing mono-biotinylated, biologically active neurotrophic factors: an essential reagent for single molecule study of axonal transport, J. Neurosci. Methods 200 (2) (2011) 121–128.
[20] X. Zhao, Y. Zhou, A.M. Weissmiller, M.L. Pearn, W.C. Mobley, C. Wu, Real-time imaging of axonal transport of quantum dot-labeled BDNF in primary neurons, JoVE (91) (2014) e51899.
[21] B. Cui, C. Wu, L. Chen, A. Ramirez, E.L. Bearer, W.-P. Li, et al., One at a time, live tracking of NGF axonal transport using quantum dots, Proc. Natl. Acad. Sci. USA 104 (34) (2007) 13666–13671.
[22] P.D. Chowdary, D.L. Che, L. Kaplan, O. Chen, K. Pu, M. Bawendi, et al., Nanoparticle-assisted optical tethering of endosomes reveals the cooperative function of dyneins in retrograde axonal transport, Sci. Rep. 5 (2015) 18059.
[23] T. Federici, J.K. Liu, Q. Teng, J. Yang, N.M. Boulis, A means for targeting therapeutics to peripheral nervous system neurons with axonal damage, Neurosurgery 60 (5) (2007) 911–918.
[24] B.K. Kaspar, J. Llado, N. Sherkat, J.D. Rothstein, F.H. Gage, Retrograde viral delivery of IGF-1 prolongs survival in a mouse ALS model, Science 301 (5634) (2003) 839–842.
[25] A. Sorkin, M. von Zastrow, Endocytosis and signalling: intertwining molecular networks, Nat. Rev. Mol. Cell Biol. 10 (9) (2009) 609–622.
[26] Y. Wong, K. Markham, Z.P. Xu, M. Chen, G.Q. Max Lu, P.F. Bartlett, et al., Efficient delivery of siRNA to cortical neurons using layered double hydroxide nanoparticles, Biomaterials 31 (33) (2010) 8770–8779.
[27] M. Schlich, F. Longhena, G. Faustini, C.M. O'Driscoll, C. Sinico, A.M. Fadda, et al., Anionic liposomes for small interfering ribonucleic acid (siRNA) delivery to primary neuronal cells: evaluation of alpha-synuclein knockdown efficacy, Nano Res. 10 (10) (2017) 3496–3508.
[28] S.A. Townsend, G.D. Evrony, F.X. Gu, M.P. Schulz, Jr RH. Brown, R. Langer, Tetanus toxin C fragment-conjugated nanoparticles for targeted drug delivery to neurons, Biomaterials 28 (34) (2007) 5176–5184.
[29] R.L. Rungta, H.B. Choi, P.J. Lin, R.W. Ko, D. Ashby, J. Nair, et al., Lipid nanoparticle delivery of siRNA to silence neuronal gene expression in the brain, Mol. Ther. Nucleic Acids 2 (12) (2013) e136.
[30] L. Zhang, Y. Xia, Y. Gui, Neuronal ApoE 4 in Alzheimer's disease and potential therapeutic targets, Front. Aging Neurosci. 15 (2023) 1199434.
[31] W.W. Liu, J. Goodhouse, N.L. Jeon, L. Enquist, A microfluidic chamber for analysis of neuron-to-cell spread and axonal transport of an alpha-herpesvirus, PLoS One 3 (6) (2008) e2382.
[32] J.W. Park, B. Vahidi, A.M. Taylor, S.W. Rhee, N.L. Jeon, Microfluidic culture platform for neuroscience research, Nat. Protoc. 1 (4) (2006) 2128–2136.
[33] H.J. Kim, J.W. Park, J.H. Byun, W.W. Poon, C.W. Cotman, C.C. Fowlkes, et al., Quantitative analysis of axonal transport by using compartmentalized and surface micropatterned culture of neurons, ACS Chem. Neurosci. 3 (6) (2012) 433–438.
[34] C.D. Lopes, C.P. Gomes, E. Neto, P. Sampaio, P. Aguiar, A.P. Pêgo, Microfluidic-based platform to mimic the in vivo peripheral administration of neurotropic nanoparticles, Nanomedicine 11 (24) (2016) 3205–3221.
[35] T. Nagendran, R.S. Larsen, R.L. Bigler, S.B. Frost, B.D. Philpot, R.J. Nudo, et al., Distal axotomy enhances retrograde presynaptic excitability onto injured pyramidal neurons via trans-synaptic signaling, Nat. Commun. 8 (2017).
[36] A. Lesniak, D. Kilinc, A. Blasiak, G. Galea, J.C. Simpson, G.U. Lee, Rapid growth cone uptake and dynein-mediated axonal retrograde transport of negatively charged nanoparticles in neurons is dependent on size and cell type, Small 15 (2) (2019) e1803758.
[37] T. Nagendran, V. Poole, J. Harris, A.M. Taylor, Use of pre-assembled plastic microfluidic chips for compartmentalizing primary murine neurons, JoVE 141 (2018) e58421.
[38] N. Katiyar, G. Raju, P. Madhusudanan, V. Gopalakrishnan-Prema, S. A. Shankarappa, Neuronal delivery of nanoparticles via nerve fibres in the skin, Sci. Rep. 11 (1) (2021) 1–13.
[39] M. Schlich, R. Palomba, G. Costabile, S. Mizrahy, M. Pannuzzo, D. Peer, et al., Cytosolic delivery of nucleic acids: the case of ionizable lipid nanoparticles, Bioeng.Transl. Med. 6 (2) (2021) e10213.
[40] S. Patel, N. Ashwanikumar, E. Robinson, Y. Xia, C. Mihai, I.I.I.J.P. Griffith, et al., Naturally-occurring cholesterol analogues in lipid nanoparticles induce

polymorphic shape and enhance intracellular delivery of mRNA, Nat. Commun. 11 (1) (2020) 983.
[41] K. Syama, Z.J. Jakubek, S. Chen, J. Zaifman, Y.Y.C. Tam, S. Zou, Development of lipid nanoparticles and liposomes reference materials (II): cytotoxic profiles, Sci. Rep. 12 (1) (2022) 18071.
[42] A. Gallud, M. Munson, K. Liu, A. Idström, H. Barriga, S. Tabaei, et al., Time evolution of PEG-shedding and serum protein coronation determines the cell uptake kinetics and delivery of lipid nanoparticle formulated mRNA, bioRxiv 2021 (08. 20) (2021) 457104.
[43] S. Maday, A.E. Twelvetrees, A.J. Moughamian, E.L. Holzbaur, Axonal transport: cargo-specific mechanisms of motility and regulation, Neuron 84 (2) (2014) 292–309.
[44] H. Nakamura, N. Yamashita, Y. Kanamaru, T. Tachibana, Y. Sekino, S. Chen, et al., Quantitative analysis of intraneuronal transport in human iPS neurons, J. Pharmacol. Sci. 128 (4) (2015) 170–178.
[45] K.M. Ori-McKenney, J. Xu, S.P. Gross, R.B. Vallee, A cytoplasmic dynein tail mutation impairs motor processivity, Nat. Cell Biol. 12 (12) (2010) 1228–1234.
[46] Y. Suzuki, H. Ishihara, Difference in the lipid nanoparticle technology employed in three approved siRNA (Patisiran) and mRNA (COVID-19 vaccine) drugs, Drug Metabol. Pharmacokinet. 41 (2021) 100424.
[47] Y. Suzuki, Y. Katsurada, K. Hyodo, Differences and similarities of the Intravenously administered lipid nanoparticles in three clinical trials: potential linkage between lipid nanoparticles and extracellular vesicles, Mol. Pharm. 20 (10) (2023) 4883–4892.
[48] K. Xu, S. Duan, W. Wang, Q. Ouyang, F. Qin, P. Guo, et al., Nose-to-brain delivery of nanotherapeutics: transport mechanisms and applications, Wiley Interdiscip. Rev.: Nanomed. Nanobiotechnol. 16 (2) (2024) e1956.
[49] R. Iqbal, S. Ahmed, G.K. Jain, D. Vohora, Design and development of letrozole nanoemulsion: a comparative evaluation of brain targeted nanoemulsion with free letrozole against status epilepticus and neurodegeneration in mice, Int. J. Pharm. 565 (2019) 20–32.
[50] D. Sharma, R.K. Sharma, N. Sharma, R. Gabrani, S.K. Sharma, J. Ali, et al., Nose-to-brain delivery of PLGA-diazepam nanoparticles, AAPS PharmSciTech 16 (2015) 1108–1121.
[51] A.K. Al Asmari, Z. Ullah, M. Tariq, A. Fatani, Preparation, characterization, and in vivo evaluation of intranasally administered liposomal formulation of donepezil, Drug Des. Dev. Ther. (2016) 205–215.
[52] W. Li, Y. Zhou, N. Zhao, B. Hao, X. Wang, P. Kong, Pharmacokinetic behavior and efficiency of acetylcholinesterase inhibition in rat brain after intranasal administration of galanthamine hydrobromide loaded flexible liposomes, Environ. Toxicol. Pharmacol. 34 (2) (2012) 272–279.
[53] D. Lee, T. Minko, Nanotherapeutics for nose-to-brain drug delivery: an approach to bypass the blood brain barrier, Pharmaceutics 13 (12) (2021) 2049.
[54] T. Ahmed, Lipid nanoparticle mediated small interfering RNA delivery as a potential therapy for Alzheimer's disease, Eur. J. Neurosci. 59 (11) (2024) 2915–2954.